On nonlinear convection in mushy layers. Part 2. Mixed oscillatory and stationary modes of convection

D. N. Riahi
Department of theoretical and Applied Mechanics

216 Talbot Laboratory, 104 South Wright Street

University of Illinois at Urbana-Champaign

Urbana, IL 61801, USA

Abstract

This paper presents part 2 of the problem of nonlinear convection in horizontal mushy layers during the solidification of binary alloys. Part 1 of the problem dealt with only the oscillatory modes of convection, which was investigated very recently (Riahi2002). In the present paper we consider particular range of the parameter values where the critical values of the scaled Rayleigh number R for the onset of oscillatory and stationary convection are sufficiently close, and we develop and analyze a nonlinear theory in such parameter regime which takes into account both stationary and oscillatory modes of convection. Under a near-eutectic approximation and the limit of large far-field temperature, we determine the weakly nonlinear solutions due to mixed oscillatory and stationary modes. Twelve new classes of these solutions, which are referred to hereafter as mixed solutions, are detected. The oscillatory component of any mixed solution depends on a parameter b, which lies in the range $|b|\leq 0.5$. The standing wave component corresponds to b=0.0, the simple travelling components correspond to |b|=0.5, and the general travelling components correspond to $0.0<|b|<0.5$. The preferred mixed solutions, which correspond to the lowest value of R, are found to be subcritical and composed of

general travelling rectangular mode and stationary hexagonal mode, where the two wave number vectors of any oscillatory rectangular cell are along two wave number vectors of a corresponding stationary hexagonal cell. In contrast to the simple type of either oscillatory solution, where the subcritical three-dimensional pattern cannot be possible, or stationary solutions, where down-hexagons with down-flow at the cells' centers and up-flow at the cells' boundaries cannot be preferred or be predicted in the domain of the experimental observation for such pattern, the preferred mixed solutions with down-flow at the cells' centers and up-flow at the cells' boundaries are predicted in the domain of the experimental observation.

1. Introduction and governing system

Very recently Riahi (2002) studied part 1 of the problem of nonlinear convection in horizontal mushy layers during the solidification of binary alloys. He analyzed the oscillatory modes of convection in particular range of the parameter values where the critical value $R_c^{(o)}$ of the scaled Rayleigh number R for the onset of oscillatory convection is distinctly lower than the critical value $R_c^{(s)}$ of R for the onset of stationary convection. His results indicated preference of supercritical simple travelling rolls over most of the studied range of the parameter values, while supercritical standing rolls could be preferred only over a rather small range of the parameter values. His detailed nonlinear study of the oscillatory modes of convection in mushy layers complemented the previous nonlinear studies of the stationary convection in mushy layers (Amberg and Homsy1993; Anderson and Worster1995).

The motivation and justification for the present investigation was due to the realization that, under the already established relevant scaling (Anderson and Worster1995, 1996), the linear system of the problem in particular range of the parameter values exhibits both oscillatory and stationary modes of convection at very close values of $R_c^{(o)}$ and $R_c^{(s)}$. Such particular range of the parameter values turns out to cover that of the available experimental results (Tait et al.1992). Hence, to determine the analytical results, which can be applicable to such range of the parameter values and, in particular, can be compared with the available experimental results (Tait et al.1992) with some confidence, the present nonlinear theory for the mixed modes of oscillatory and stationary convection was needed to be developed and analyzed.

The present theory was first motivated by the work due to Busse and Riahi (1988) for the mixed-mode patterns of bifurcations from spherically symmetric basic states. These authors determined a number of new patterns which are likely to occur in bifurcations from spherically symmetric basic states when two neighboring degrees l and l^* of spherical harmonics yield nearly the same lowest value of the control parameter R. Their preferred solutions were based on the assumption of the type adopted before by Busse (1975) that the solution, which exists at the lowest value of the control parameter R, is the physically preferred solution. This assumption can follow from the stability results (Busse1967; Riahi1983). In the present paper we follow Busse (1975) and Busse and Riahi (1988) and adopt the same criterion to determine the preferred solutions.

We consider a binary alloy melt that is cooled from below and is solidified at a constant speed V_0. Following Amberg and Homsy (1993) and Anderson and Worster (1995), we consider mushy layer of thickness d adjacent and above the solidification

front to be physically isolated from the overlying liquid and underlying solid zones. The overlying liquid is assumed to have a composition $C_0 > C_e$ and temperature $T_\infty > T_L(C_0)$ far above the mushy layer, where C_e is the eutectic composition, $T_L(\tilde{C})$ is the liquidus temperature of the alloy and $\tilde{C}$ is the composition. It is then assumed that the horizontal mushy layer is bounded from above and below by rigid and isothermal boundaries. We consider the solidification system in a moving frame of reference $o\tilde{x}\tilde{y}\tilde{z}$, whose origin lies on the solidification front and translating at the speed V_0 with the solidification front in the positive $\tilde{z}$-direction. The reader is referred to part 1 of the present problem (Riahi2002) for the motivation and justification in using the Amberg and Homsy (1993) type of model for the present study.

The governing system of equations and the boundary condition for the present problem were already provided with some details in Riahi (2002). Thus, only the final version of the governing system is given below

$$\nabla^2[K(\phi_B+\varepsilon\phi)\Delta_2 V]+(\partial/\partial z)[\mathbf{\Omega}V.\nabla K(\phi_B+\varepsilon\phi)]-R\Delta_2\theta=0, \tag{1a}$$

$$(\partial/\partial t-\delta\partial/\partial z)(-\theta+S\phi/\delta)+R\,(d\theta_B/dz)\Delta_2 V+\nabla^2\theta=\varepsilon R\mathbf{\Omega}V.\nabla\theta, \tag{1b}$$

$$(\partial/\partial t-\delta\partial/\partial z)[(-1+\phi_B)\theta+\theta_B\phi+\varepsilon\phi\theta-C\phi/\delta]+R\,(d\theta_B/dz)\Delta_2 V=\varepsilon R\mathbf{\Omega}V.\nabla\theta, \tag{1c}$$

$$\theta=V=0 \text{ at } \quad z=0, \tag{1d}$$

$$\theta=V=\phi=0 \quad \text{at} \quad z=1, \tag{1e}$$

where

$$\Delta_2\equiv \partial^2/\partial x^2+\partial^2/\partial y^2.$$

The exact definitions of all the symbols used in (1a)-(1e) are given in part 1 (Riahi2002). However, to make the present paper somewhat self-independent from its part 1, these definitions are briefly provided here. The dimensionless scaled dependent variables are

the poloidal function V for the scaled velocity vector, basic composition or equivalently basic temperature θ_B, deviation θ of temperature or equivalently of composition from its basic state, basic solid fraction ϕ_B and deviation ϕ of solid fraction from its basic state. The dimensionless scaled spatial variables are x, y and z. The dimensionless scaled variable for time is t, $\boldsymbol{\Omega}\equiv\nabla\times\nabla\times\mathbf{z}$, $\mathbf{z}$ is a unit vector in the positive z-direction, $K(\tilde{\phi})\equiv\Pi(0)/\Pi(\tilde{\phi})$, $\tilde{\phi}=\phi_B+\varepsilon\phi$, ε is the perturbation amplitude and $\Pi(\phi)$ is the permeability of the porous medium. The non-dimensional parameters of the problem are the depth of the mushy layer $\delta=dV_0/k$, the scaled Rayleigh number $R=[\delta\beta\Delta C\, g\, \Pi(0)/(V_0\nu)]^{0.5}$, the scaled Stefan number $S=\delta L/(C_L\Delta T)$ and the scaled concentration ratio $C=\delta(C_s-C_0)/\Delta C$. Here k is the thermal diffusivity, $\Delta C=C_0-C_e$, $\Delta T=T(C_0)-T_e$, T_e is the eutectic temperature, g is acceleration due to gravity, $\beta=\beta^*-\Gamma\alpha^*$, where α^* and β^* are the coefficients for the heat and solute, respectively, Γ is the slope of the liquidus, C_L is the specific heat per unit volume, L is the latent heat of solidification per unit volume, C_s is the composition of the solid-phase forming the dendrites and ν is the kinematic viscosity. The expressions for the basic state quantities are already given in the part 1 and will not be repeated here. As in part 1, the following expansion for $K(\tilde{\phi})$ is assumed:

$$K(\tilde{\phi})=1+K_1\tilde{\phi}+K_2\tilde{\phi}^2+\ldots, \tag{2}$$

where K_1 and K_2 are constant. The small parameters ε and δ are assumed to satisfy the following condition:

$$\varepsilon<<\delta<<1, \tag{3}$$

which the same condition used in part 1.

2. Weakly nonlinear analysis and solutions

In this section we do a weakly nonlinear analysis, based on a double-series expansions in powers of δ and ε. As in part 1, we first make a formal asymptotic expansion in ε and then at each order in ε make a formal asymptotic expansion in δ. Since we investigate both steady and oscillatory modes of convection, the appropriate expansions are for the dependent variables of the perturbation system (1), R and the frequency ω for the oscillatory modes of convection. These expansions are already provided in part 1 but will be given briefly below to make the present paper somewhat self explanatory to the reader

$$(V, \theta, \phi, R, \omega)=[(V_{00}+\delta V_{01}+....), (\theta_{00}+\delta\theta_{01}+....), (\phi_{00}+\delta\phi_{01}+....), (R_{00}+\delta R_{01}+....), (\omega_{00}+\delta\omega_{01}+....)]+\varepsilon[(V_{10}+\delta V_{11}+....), (\theta_{10}+\delta\theta_{11}+....), (\phi_{10}+\delta\phi_{11}+....), (R_{10}+\delta R_{11}+....), (\omega_{10}+\delta\omega_{11}+....)]+.... \quad (4)$$

2.1. Linear analysis

Upon inserting (4) into (1a)-(1e) and disregarding the nonlinear terms, we find the linear problem whose analysis for the oscillatory modes (Riahi2002) was done in direct analogy to that carried out by Anderson and Worster (1995) for the stationary modes. Hence, no details will be provided here and, instead, the main results on the neutral boundary are given below first for the oscillatory modes and then for the stationary modes.

We consider first the oscillatory modes for the linear problem. At order $1/\delta$ we find $\omega_{00}=0$. At order δ^0 we find

$$V_{00}^{(o)}=[(\pi^2+a^2)/(R_{00}a^2G)]\sin(\pi z)\sum_m{}^{M}{}_{=-M} (A_m^{+}\,\eta_m^{+}+ A_m^{-}\,\eta_m^{-}),\ G\equiv 1+S/C, \quad (5a)$$

$$\theta_{00}^{(o)} = - \sin(\pi z)\sum_m{}^{M}{}_{=-M} (A_m^{+}\eta_m^{+} + A_m^{-}\eta_m^{-}), \quad (5b)$$

$$\phi_{00}^{(o)} = \sum_m{}^{M}{}_{=-M} [f_m(z)A_m^{+}\eta_m^{+} + f_m^{*}(z)A_m^{-}\eta_m^{-}], \ \eta_m^{\pm} \equiv \exp[i(\mathbf{a}_m^{(o)}.\mathbf{r} \pm S_m\omega_{01}t)], \quad (5c)$$

$$R_{00}^{(o)} = \{[\pi^2+(a^{(o)})^2]^2/[(a^{(o)})^2G]\}^{0.5}, \quad (5d)$$

where

$$f_m(z) = \{- 2\pi^3/[CG(\pi^2 - \omega_{01}{}^2)]\}\{i\,\omega_{01}S_m/\pi)\sin(\pi z) + \cos(\pi z) + \exp[i\,\omega_{01}S_m(z-1)]\} \quad (5e)$$

and

$$S_m = 1 \text{ for } m>0 \text{ and } -1 \text{ for } m<0. \quad (5f)$$

Here the quantities with a superscript 'o' represent those for the oscillatory modes, i is the pure imaginary number ($i \equiv \sqrt{-1}$), subscript 'm' takes only non-zero integer values from -M to M, M is a positive integer, **r** is the position vector, and the horizontal wave number vectors $\mathbf{a}_m^{(o)}$ satisfy the properties

$$\mathbf{a}_m^{(o)}.\mathbf{z} = 0, \ |\mathbf{a}_m^{(o)}| = a^{(o)}, \ \mathbf{a}_{-m}^{(o)} = -\mathbf{a}_m^{(o)}. \quad (6)$$

The coefficients A_m^{+} and A_m^{-} satisfy the conditions

$$\sum_m{}^{M}{}_{=-M} (|A_m^{+}|^2 + |A_m^{-}|^2) = 2, \ A_m^{\pm *} = A_{-m}^{\pm}, \quad (7)$$

where the asterisk indicates the complex conjugate. Minimizing the expression for $R_{00}^{(o)}$, given in (5d), with respect to the wave number $a^{(o)}$, we find

$$R_{00c}^{(o)} = 2\pi/\sqrt{G}, \ a_c^{(o)} = \pi. \quad (8)$$

We now consider the stationary modes for the linear problem. At the lowest order δ^0 we find

$$V_{00}^{(s)} = [1/(\pi\sqrt{G})]\sin(\pi z)\sum_n{}^{N}{}_{=-N} (A_n\,\eta_n), \ \eta_n \equiv \exp(i\mathbf{a}_n^{(s)}.\mathbf{r}) \quad (9a)$$

$$\theta_{00}^{(s)} = -\sin(\pi z)\sum_n{}^{N}{}_{=-N} (A_n\eta_n), \quad (9b)$$

$$\phi_{00}^{(s)} = [-2\pi/(CG)][1+\cos(\pi z)]\sum_n{}^{N}{}_{=-N} (A_n\eta_n), \quad (9c)$$

$$R_{00}^{(s)}=\{[\pi^2+(a^{(s)})^2]^2/[(a^{(s)})^2G]\}^{0.5}. \tag{9d}$$

Here the quantities with a superscript 's' represent those for the stationary modes, subscript 'n' takes only non-zero integer values from –N to N, N is a positive integer, and the horizontal wave number vectors $\mathbf{a}_n^{(s)}$ satisfy the properties

$$\mathbf{a}_n^{(s)}.\mathbf{z}=0,\ |\mathbf{a}_n^{(s)}|=a^{(s)},\ \mathbf{a}_{-n}^{(s)}=-\mathbf{a}_n^{(s)}. \tag{10}$$

The coefficients A_n satisfy the conditions

$$\sum_{n=-N}^{N}|A_n|^2=1,\ A_n^*=A_{-n}. \tag{11}$$

Minimizing the expression for $R_{00}^{(s)}$, given in (9d), with respect to the wave number $a^{(s)}$, we find

$$R_{00c}^{(s)}=2\pi/\sqrt{G},\ a^{(s)}=\pi. \tag{12}$$

It turns out, as will be presented and discussed later in this paper, that for all the values of parameters investigated so far, the critical values $R_c^{(o)}$ and $R_c^{(s)}$ of R for the oscillatory and stationary modes, respectively, always satisfy the condition

$$R_c^{(o)}<R_c^{(s)}, \tag{13}$$

and the difference $(R_c^{(s)}-R_c^{(o)})$ is small and decreases with decreasing $G_t\equiv(G-1)/(CG^2)$. For sufficiently small G_t, we designate this difference by $\lambda_1\varepsilon$ ($\lambda_1\ \varepsilon>0$), where λ_1 is a constant of order one for a given values of the parameters. Following Busse and Riahi (1988) and in the limit of sufficiently small G_t, we superimpose the stationary solution on the most critical oscillatory solution in the order δ^0 and take into account of $\lambda_1\varepsilon$ in the order-ε system to be analyzed later in this paper. Hence, at order δ^0 we have the following mixed solution

$$(V_{00},\theta_{00},\phi_{00})=[V_{00}^{(o)},\theta_{00}^{(o)},\phi_{00}^{(o)}]+B[V_{00}^{(s)},\theta_{00}^{(s)},\phi_{00}^{(s)}], \tag{14}$$

where B is an arbitrary constant.

At order δ we find the solutions $V_{01}^{(o)}$, $\theta_{01}^{(o)}$, $\phi_{01}^{(o)}$, $V_{01}^{(s)}$, $\theta_{01}^{(s)}$ and $\phi_{01}^{(s)}$. The solvability condition at this order for the system of the oscillatory modes yield

$$R_{01}^{(o)}=[\pi K_1 /(2C\sqrt{G})]+2\pi G_t\sqrt{G}[1/4+ \pi^2(1+\cos\omega_{01})/(\pi^2 -\omega_{01}^2)^2], \quad (15a)$$

$$1+[2\pi^2 G_t/(\pi^2-\omega_{01}^2)][1-2\pi^2\sin\omega_{01}/(\pi^2\omega_{01}-\omega_{01}^3)]=0, \quad (15b)$$

while that for the system of the stationary modes yield

$$R_{01}^{(s)}=[\pi K_1/(2C\sqrt{G})]+2\pi G_t\sqrt{G}(1/4+2/\pi^2). \quad (15c)$$

The critical $R_c^{(o)}$ and $R_c^{(s)}$ for the onset of oscillatory and stationary convection, to order δ^2, can then be written as

$$R_c^{(o)} =(2\pi/\sqrt{G})+\delta R_{01}^{(o)} +O(\delta^2),\ R_c^{(s)}=(2\pi/\sqrt{G})+\delta R_{01}^{(s)}+O(\delta^2). \quad (16)$$

2.2. General nonlinear analysis

Next, we analyze the nonlinear problem. At order ε/δ, we find $\omega_{00}=0$. At order ε the system (1a)-(1e) can be reduced to the form given by (A1) in Appendix. The solvability conditions for the nonlinear system require us the following two sets of special solutions of the linear system

$$(V_{00n}^{(o)}, \theta_{00n}^{(o)})=[1/(\pi\sqrt{G}), -1]\sin(\pi z)(A_n^+ \eta_n^+ +A_n^- \eta_n^- +C.C.), \quad (17a)$$

$$(V_{00n}^{(s)}, \theta_{00n}^{(s)})=[1/(\pi\sqrt{G}), -1](A_n \eta_n+ C.C.), \quad (17b)$$

where 'C.C.' indicates complex conjugate of the preceding expression. There is no need to consider special linear solutions for ϕ since it was possible to reduce the governing nonlinear system to a form where only (17) will be needed to form the necessary solvability conditions.

Multiplying the first equation in (A1) by $GV_{00n}^{(o)}$ ($GV_{00n}^{(s)}$), the second equation in (A1) by $\theta_{00n}^{(o)}$ ($\theta_{00n}^{(s)}$) , adding, applying the boundary conditions, averaging over the whole layer and taking a time average over period $2\pi/\omega_{01}$ yield two sets of equations,

which are reduced to those given by (A2a) and (A2b) in the appendix. Using (A2a) and (A2b), we have detected twelve major new classes of solutions for which R_{10} is non-zero and can represent six classes of subcritical convection cases, where $\varepsilon R_{10} < 0$, and six classes of supercritical convection cases, where $\varepsilon R_{10} > 0$. The analysis and the solutions for these classes are presented in the following sub-sections.

2.3. Nonlinear analysis for simple travelling-steady mixed class of modes

We consider the simple travelling component of the mixed solutions to be in the form of right-travelling modes where the phase velocity of each mode is in the direction of the component of the mode's wave vector along **r**. For the case of simple travelling component of the mixed solutions in the form of left-travelling modes where the phase velocity of each mode is in the direction opposite to that of the component of the mode's wave vector along **r**, we find identical results regarding the value of R_{10} for each detected solution. Hence, the present analysis is presented here only for the case of simple travelling component of the mixed solutions in the form of right-travelling modes. The right-travelling-steady mixed solutions of (A2a)-(A2b) are given below in the so-called 'semi-regular' case, in which scalar product between any one of the **a**-vectors and its two neighbouring **a**-vectors assumes the constant values α_1 and α_2 (Busse 1967; Riahi 2002):

$$|A_1^+|=...=|A_M^+|=0,\ |A_1^-|^2=...=|A_M^-|^2=1/M,\ |A_1|^2=...=|A_N|^2=1/(2N), \tag{18a}$$

$$R_{10}=B\sum_{l,p}\{K_1\pi^4(H_p^*)/[CG(2GN)^{0.5}(\pi^2-\omega_{01}^2)]-3K_1\pi^2/[2G(2GN)^{0.5}]\}(1+\psi_{lp}^{(m)})(<\eta_l\,\eta_p^-\,\eta_1^->+<\eta_l\,\eta_p^-\,\eta_{-1}^->), \tag{18b}$$

$$(R_{10}+\lambda_1)B=\{K_1\pi^4(2N/G)^{0.5}/[MCG(\pi^2-\omega_{01}^2)]\}\sum_{l,p}{}^{M}{}_{=-M}(1+\psi_{lp}^{(o)})H_p^*(<\eta_1\,\eta_l^-\,\eta_p^->+<\eta_{-1}\,\eta_l^-\,\eta_p^->)-B^2\{3K_1\pi^2/[2CG(2GN)^{0.5}]\}\sum_{l,p}{}^{N}{}_{=-N}(1+\psi_{lp}^{(s)})(<\eta_l\,\eta_p\eta_1>+<\eta_l\,\eta_p\eta_{-1}>), \tag{18c}$$

where the summation in the right-hand-side in (18b) runs for l from –N to N and for p from –M to M.

Using (18a)-(18c), we looked for new type of mixed solutions for which R_{10} can be non-zero and evaluated terms in the right-hand-side in these equations. These terms involve integrals of the form $<\eta_l\, \eta_p^-\, \eta_n^->$, $<\eta_l^-\, \eta_p^-\, \eta_n>$ and $<\eta_l\, \eta_p\, \eta_n>$ (n= -1,1), which were computed for six detected mixed solutions. To describe these solutions, we write (18a) and (18b) in the form

$$R_{10}=C_1B,\ (R_{10}+\lambda_1)B=C_2+C_3B^2, \tag{19}$$

where the coefficients C_i (i =1, 2, 3), which are functions of C, G, K_1 and ω_{01}, are designated by $C_i^{(j)}$ for each of the j-solutions (j=1,..., 6). The expressions for these coefficients are given by (A3a)-(A3f) in the appendix. The detected six mixed solutions are described briefly as follows. The mixed solution for j=1 is called simple travelling hexagons-steady hexagons. It corresponds to the case N=M=3 where all the wave number vectors of each steady hexagonal cell are along all the wave number vectors of a corresponding simple travelling hexagonal cell. The mixed solution for j=2 is called simple travelling rectangles-steady hexagons. It corresponds to the case N=3 and M=2 where all the wave number vectors of each simple travelling rectangular cell are along a subset of the wave number vectors of a corresponding steady hexagonal cell. Hence, the angles between any one of the $\mathbf{a}^{(o)}$-vectors of the simple travelling rectangular component of the mixed solution with its two neighbouring $\mathbf{a}^{(o)}$-vectors are 60° and 120° or vice versa. The mixed solution for j=3 is called simple travelling hexagons-steady rectangles. It corresponds to the case N=3 and M=2 where all the wave number vectors of each steady rectangular cell are along a subset of the wave number vectors of a corresponding

simple travelling hexagonal cell. Hence, the angles between any one of the $\mathbf{a}^{(s)}$-vectors of the steady rectangular component of the mixed solution with its two neighbouring $\mathbf{a}^{(s)}$-vectors are 60° and 120° or vice versa. The mixed solution for j=4 is called simple travelling rectangles-steady rectangles. It corresponds to the case N=M=2 where one wave number vector of any steady rectangular cell makes 120° angle with each of the two wave number vectors of a corresponding simple travelling rectangular cell. In addition, the angles between any one of the wave number vectors of either steady or simple travelling rectangular component with its two neighbouring wave number vectors should be 60° and 120° or vice versa. The mixed solution for j=5 is called simple travelling hexagons-steady rolls. It corresponds to the case N=1 and M=3 where the wave number vector of any roll makes 120° angle with each of two neighbouring wave number vectors of a corresponding simple travelling hexagonal cell. The mixed solution for j=6 is called simple travelling rectangles-steady rolls. It corresponds to the case N=1 and M=2 where the wave number vector of any roll make 120 angle with each of the two wave number vectors of a corresponding simple travelling rectangular cell. In addition, the angles between any wave number vector of the simple travelling rectangles with its two neighbouring wave number vectors should be 120° and 60° or vice versa. These six solutions are called here solutions numbers 1 through 6.

Using (4) and the introduction of λ_1 provided in the sub-section 2.1, we have to order ε^2

$$\lambda_1=L_1R_{10},\ L_1\equiv[(R_c^{(s)}-R_c^{(o)})/(R-R_c^{(o)})]. \tag{20}$$

Using (20) in (19), we find

$$[R_{10}^{(j)}]^2=C_2^{(j)}\ [C_1^{(j)}]^2\ /[C_1^{(j)}-C_3^{(j)}+L_1C_1^{(j)}],\ B^{(j)}=R_{10}^{(j)}/C_1^{(j)}, \tag{21}$$

where quantities with superscript 'j' represent those for the solution number j. Here j runs from 1 to 6 for the six solutions.

2.4. Nonlinear analysis for standing wave-steady mixed class of modes

We now consider the oscillatory component of the mixed solutions to be in the form of standing waves where $A_n^+=A_n^-$ for every n. The standing wave-steady mixed solutions of (A2a)-(A2b) are given below in the semi-regular case:

$$|A_1^{\pm}|^2=...=|A_M^{\pm}|^2=1/(2M),\ |A_1|^2=...=|A_N|^2=1/(2N), \tag{22a}$$

$$R_{10}=B\sum_{l,p}\{K_1\pi^4(H_p)/[2CG(2GN)^{0.5}(\pi^2-\omega_{01}^2)]-3K_1\pi^2/[4CG(GN)^{0.5}]\}(1+\psi_{lp}^{(m)})(<\eta_l\eta_p^+\eta_1^+>+<\eta_l\eta_p^+\eta_{-1}^+>+<\eta_l\eta_p^+\eta_1^->+<\eta_l\eta_p^+\eta_{-1}^->)+B\sum_{l,p}\{K_1\pi^4(H_p^*)/[2CG(2GN)^{0.5}(\pi^2-\omega_{01}^2)]-3K_1\pi^2/[4CG(GN)^{0.5}]\}(1+\psi_{lp}^{(m)})(<\eta_l\eta_p^-\eta_1^+>+<\eta_l\eta_p^-\eta_{-1}^+>+<\eta_l\eta_p^-\eta_1^->+<\eta_l\eta_p^-\eta_{-1}^->), \tag{22b}$$

$$(R_{10}+\lambda_1)B=\{K_1\pi^4(2N/G)^{0.5}/[2CGM(\pi^2\omega_{01}^2)]\}\sum_{l,p}{}^{M}{}_{=M}(1+\psi_{lp}^{(o)})[H_p(<\eta_l^+\eta_p^+\eta_1>+<\eta_l^+\eta_p^+\eta_{-1}>+<\eta_l^-\eta_p^+\eta_1>+<\eta_l^-\eta_p^+\eta_{-1}>)+H_p^*(<\eta_l^+\eta_p^-\eta_1>+<\eta_l^+\eta_p^-\eta_{-1}>+<\eta_l^-\eta_p^-\eta_1>+<\eta_l^-\eta_p^-\eta_{-1}>)]-B^2\{3K_1\pi^2/[2CG(2GN)^{0.5}]\}\sum_{l,p}{}^{N}{}_{=-N}(1+\psi_{lp}^{(s)})(<\eta_l\eta_p\eta_1>+<\eta_l\eta_p\eta_{-1}>), \tag{22c}$$

where the summations in the right-hand-side in (22b) run for l from –N to N and for p from –M to M.

Using (22a)-(22c), we looked for new types of mixed solutions for which R_{10} can be non-zero and evaluated terms in the right-hand-sides of (22b) and (22c). These terms involve integrals of the form $<\eta_l^{\pm}\eta_p^{\pm}\eta_n>$, $<\eta_l\eta_p^{\pm}\eta_n^{\pm}>$ and $<\eta_l\eta_p\eta_n>$ (n =-1,1). These integrals and the terms in (22b) and (22c) were computed for six detected mixed solutions for which (19) hold, where the coefficients C_i (i=1, 2, 3) are now designated by $C_i^{(j+6)}$ for these six solutions (j+6=7, 8, 9, 10, 11, 12). These six solutions are called here solutions numbers 7 through 12. The descriptions of the solutions numbers 7 through 12 are,

respectively, the same as those for the solutions numbers 1 through 6 presented in the last sub-section, provided the simple travelling component is replaced by standing wave component. The result (21) hold here for these 6 solutions (j=7,..., 12), where the expressions for $C_i^{(j)}$ are given by (A4a)-(A4f) in the appendix.

2.5. Nonlinear analysis for general travelling-steady mixed class of modes

In this sub-section we consider the oscillatory component of the mixed solutions to be in the form of general travelling waves of the types introduced in part 1 (Riahi2002). The general travelling-steady mixed solutions of (A2a)-(A2b) are given below in the semi-regular case:

$$A_1^+=...=A_M^+=[(0.5-b)/M]^{0.5},\ A_1^-=...=A_M^-=[(0.5+b)/M]^{0.5},\ |A_1|=...=|A_N|=1/(2N), \tag{23a}$$

$$R_{10}=B\sum_{l,p}\{K_1\pi^4/[CG\,H_p(2NG)^{0.5}(\pi^2-\omega_{01}^2)]-3K_1\pi^2/[2CG(2GN)^{0.5}]\}(1+\psi_{lp}^{(m)})[(0.5-b)(<\eta_l\,\eta_p^+\eta_1^+>+<\eta_l\,\eta_p^+\eta_{-1}^+>)+(0.25-b^2)^{0.5}(<\eta_l\,\eta_p^+\eta_1^->+<\eta_l\,\eta_p^+\eta_{-1}^->)]+B\sum_{l,p}\{K_1\pi^4/[CG\,H_p^*(2NG)^{0.5}(\pi^2-\omega_{01}^2)]-K_1\pi^2/[2CG(2GN)^{0.5}]\}(1+\psi_{lp}^{(m)})[(0.25-b^2)^{0.5}(<\eta_l\,\eta_p^-\,\eta_1^+>+<\eta_l\,\eta_p^-\,\eta_1^+>)+(0.5+b)(<\eta_l\,\eta_p^-\,\eta_1^->+<\eta_l\,\eta_p^-\,\eta_{-1}^->)], \tag{23b}$$

$$(R_{10}+\lambda_1)B=\{K_1\pi^4(2N/G)^{0.5}/[CGM(\pi^2-\omega_{01}^2)]\}\sum_{l,p}{}^{M}{}_{=-M}(1+\psi_{lp}^{(o)})\{H_p[(0.5-b)(<\eta_l^+\eta_p^+\eta_1>+<\eta_l^+\eta_p^+\eta_{-1}>)+(0.25-b^2)^{0.5}(<\eta_l^-\,\eta_p^+\eta_1>+<\eta_l^-\,\eta_p^+\eta_{-1}>)]+H_p^*[(0.25-b^2)^{0.5}(<\eta_l^+\eta_p^-\,\eta_1>+<\eta_l^+\eta_p^-\,\eta_{-1}>)+(0.5+b)(<\eta_l^-\,\eta_p^-\,\eta_1>+<\eta_l^-\,\eta_p^-\,\eta_{-1}>)]\}-B^2\{3K_1\pi^2/[2CG(2GN)^{0.5}]\}\sum_{l,p}{}^{N}{}_{=-N}(1+\psi_{lp}^{(s)})(<\eta_l\,\eta_p\eta_1>+<\eta_l\,\eta_p\eta_{-1}>), \tag{23c}$$

where the constant b is in the range

$$|b|<0.5 \tag{23d}$$

and is the parameter for the general travelling component, whose specific value in the range (23d) provides particular general travelling component of the mixed solutions. The

summations in the right-hand-side in (23b) run for l from –N to +N and for p from –M to M.

Using (23a)-(23c), we looked for new types of mixed solutions for which R_{10} can be non-zero and evaluated terms in the right-hand-sides of (23b) and (23c). These terms involve integrals of the form $<\eta_l\, \eta_p^{\pm}\, \eta_n^{\pm}>$, $<\eta_l^{\pm}\, \eta_p^{\pm}\, \eta_n>$ and $<\eta_l\, \eta_p\, \eta_n>$ (n= -1, 1). These integrals and terms in (23b)-(23c) were computed for 6 detected mixed solutions for which (19) hold, where the coefficients C_i (i=1, 2, 3) are now designated by $C_i^{(j)}$ for these six solutions (j=13, 14, 15, 16, 17, 18). These 6 solutions are called here solutions numbers 13 through 18. The descriptions of the solutions numbers 13 through 18 are, respectively, the same as those for the solutions numbers 1 through 6 presented in the sub-section 2.3, provided the simple travelling component for each solution is replaced by general travelling component. The result (21) hold here for these 6 solutions (j=13,..., 18), where the expressions for $C_i^{(j)}$ are given by (A5a)-(A5f) in the appendix.

3. Results and discussion

3.1. Linear problem

The linear system with its eigenvalue problems for both oscillatory and stationary modes, which led to the results (5)-(17), are in general, functions of the two composite parameters G and G_t. As discussed in part 1, these two parameters, which can represent the scaled Stefan number S and the scaled compositional ratio C in a composite manner, are found to be relevant for the present mixed oscillatory-stationary system. Hence, the results presented in the present paper are given for given values of G and G_t. As explained earlier in the section 2, the present mixed system is most realistic for

sufficiently small values of G_t. It should also be noted that for the experimental results due to Tait et al. (1992), the values of G and G_t can be evaluated to be about $G \approx 1.25$ and $G_t \approx 0.008$, so that G_t can, indeed, be quite small experimentally, as well. The results presented in this paper are for the range of values $0.833 \le S \le 6.667$ and $3.333 \le C \le 26.667$, which correspond to G=1.25 and $0.006 \le G_t \le 0.048$. The results for the solution of (15b) for the frequency ω_{01} of the oscillatory component of the mixed solutions as function of small values of G_t ($0.006 \le G_t \le 0.048$) are presented in Figure 1. As can be seen from this figure, ω_{01} increases with G_t and has a higher rate of increase with respect to G_t in the range $G_t < 0.01$. As (15b) indicates, ω_{01} is independent of K_1 and G. The results for $R_c^{(o)}$ and $R_c^{(s)}$ as functions of G_t and for given values $K_1=1.0$, G=1.25 and $\delta=0.2$ are given in Figure 2. Similar to the calculation made in part 1, here, and thereafter, the value of $\delta=0.2$ is chosen to evaluate the critical values of the scaled Rayleigh number and other quantities whose values may depend on δ. It can be seen from this figure that both $R_c^{(o)}$ and $R_c^{(s)}$ are stabilizing with respect to G_t in the sense that both increase with G_t. The value of $R_c^{(o)}$ is consistently smaller than that for $R_c^{(s)}$ but $[R_c^{(s)}-R_c^{(o)}]$ decreases with decreasing G_t, and, as stated before, the present theory is most realistic in the range for G_t where $[R_c^{(s)}-R_c^{(o)}]$ is sufficiently small. In the whole range for G_t shown in the figure 2 the values of $[R_c^{(s)} - R_c^{(o)}]$ can be considered to be sufficiently small since these values are less than 1/500 of the values of either $R_c^{(s)}$ or $R_c^{(o)}$. These small values for $[R_c^{(s)}-R_c^{(o)}]$ are made sure to be consistent with the small values of the equivalent quantity $\varepsilon\lambda_1$ evaluated later for the nonlinear results. Our additional calculated data, as well as (16), indicated that both $R_c^{(o)}$ and $R_c^{(s)}$ are destabilizing and stabilizing with respect to G and K_1, respectively, in the sense that both decrease with increasing G and decreasing K_1.

The physical meaning of the effects of G and G_t on the linear system has already been explained in part 1 for the oscillatory modes and such explanation was found to be valid also for the mixed modes studied here. The stabilizing effect on the linear system when K_1 increases, is consistent with the physical role played by K_1 since the permeability of the mushy layer decreases with increasing K_1.

3.2. Nonlinear problem

An important quantity due to the nonlinear effects is the coefficient R_{10}, which turns out to be non-zero for a number of mixed solutions within several classes of such solutions. The coefficient R_{10} is the leading contribution to the change in R required to obtain given finite amplitude ε for a nonlinear solution. Using the expansion for R given in (4), the amplitude of convection can be found to be of order

$$\varepsilon=[R-R_c^{(o)}]/R_{10}. \tag{24}$$

The sign of εR_{10} determines whether the mixed solution exists for values of R above or below $R_c^{(o)}$. The convection due to mixed modes can be supercitical for

$$\varepsilon R_{10}>0 \tag{25a}$$

and subcritical for

$$\varepsilon R_{10}<0. \tag{25b}$$

For all the mixed solutions detected in the present problem where R_{10} is non-zero, it was found that the cells' patterns, due to various joint oscillatory and stationary modes, referred to here as mixed patterns, behave essentially like that of hexagons in the sense of contributing non-zero terms in the expression for R_{10}. For supercitical case, up-mixed patterns, with up-flow at the cells' centers and down-flow at the cells' boundaries, correspond to the case where

$$\varepsilon>0 \text{ and } R_{10}>0, \tag{26a}$$

while down-mixed patterns, with down-flow at the cells' centers and up-flow at the cells' boundaries, correspond to the case where

$$\varepsilon<0 \text{ and } R_{10}<0. \tag{26b}$$

For subcritical case, up-mixed patterns correspond to the case

$$\varepsilon>0 \text{ and } R_{10}<0, \tag{26c}$$

while down-mixed patterns correspond to the case

$$\varepsilon<0 \text{ and } R_{10}>0. \tag{26d}$$

In the present investigation we are interested to study the preferred mixed solutions, which correspond to the lowest value of R. These types of mixed solutions need satisfy either (26c) or (26d) and should correspond to the largest values of $|R_{10}|$.

Using (21), we calculated the values of R_{10} for relevant values of G and G_t, where the mixed solutions are the most realistic ones. We found that the preferred solutions with largest values of $|R_{10}|$ are in the form of general travelling rectangle- steady hexagons, where, depending on the values of G_t and R, the general travelling mode component can be preferred for some particular values of b near 0.5. It should be noted that (21) yield two solutions $\pm R_{10}$, provided the right-hand-side in (21) is positive. Otherwise, no real solution is possible. The admittance of two solutions $\pm R_{10}$ in the present problem opens the possibility for the preference of subcritical down-mixed pattern and is in contrast to simple solutions in the form of either oscillatory modes alone (Riahi2002), where no subcritical solution is possible, or stationary modes alone (Amberg and Homsy 1993), where no subcritical down-hexagons is possible.

Some typical results about the effect of G_t are presented in Figures 3 and 4 for R_{10} of the preferred solutions in the form of subcritical and down-mixed pattern, due to general travelling rectangles-steady hexagons, versus G_t for G=1.25, K_1=1.0 and different excess values of $R_c^{(o)}$ over R in the nonlinear regime. Figure 3 presents the results for the case of excess value 1.0 of $R_c^{(o)}$ over R. The solid line corresponds to the case of b=0.45, while the dashed line corresponds to the case b=0.46. It is seen from this figure that over the range of values shown for G_t, the pattern with the oscillatory component corresponding to b=0.45 is the preferred one for G_t<0.009, while the pattern with the oscillatory component corresponding to b=0.46 is the preferred one for G_t>0.009. The value of R_{10} for either cases of b=0.45 and 0.46 increases with G_t, provided G_t values are not too small. For sufficiently small G_t, R_{10} decreases first before increases with G_t in the case of b=0.45, while R_{10} has a sharp increase and then a moderate increase and decrease with increasing G_t. Figure 4 presents the results for the case of excess value 0.1 of $R_c^{(o)}$ over R. The solid line corresponds to the case of b=0.44, while the dashed line corresponds to the case b=0.45. It is seen from this figure that over the range of values shown for G_t, the pattern corresponding to b=0.44 is the preferred one for G_t<0.007, while the pattern corresponding to b=0.45 is the preferred one for G_t >0.007. The value of R_{10} for either cases of b=0.44 and 0.45 increases with G_t over the whole range of G_t, except for a slight decrease in the range 0.008<G_t<0.01 for the solution corresponding to b=0.45.

We also calculated the values of R_{10} for the preferred solutions and for the cases where instead of given excess values of $R_c^{(o)}$ over R in the nonlinear regime, some given values of R in the subcritical regime are provided. Some typical results are presented in Figures

5 and 6 for R_{10} of the preferred solutions in the form of subcritical and down-mixed pattern, due to general travelling rectangles-steady hexagons, versus G_t for G=1.25, K_1=1.0 and different values of R in the subcritical regime. Figure 5 presents the results for R=4.6, which is compatible with the regime for R given in the figure 3 as can be checked from the $R_c^{(o)}$-data given in the figure 2. The solid line corresponds to the case b=0.45, while the dashed line corresponds to the case b=0.46. It can be seen that the results for R_{10} given in the figure 5 are very close to the corresponding ones given in the figure 3, except for a slight wider range of the preferred solution for b=0.46 in the case of shown in the figure 5 as compared to the corresponding one in the figure 3. Figure 6 presents the results for R=5.5, which is compatible with the regime for R given in the figure 4. However, here the solid line corresponds to b=0.45, and the dashed line corresponds to b=0.46. Thus, there are significant differences between the results given in the figures 4 and 6. As can be seen from the figure 6, the solution for b=0.45 is the preferred one in the range G_t<0.016, while the solution for b=0.46 is the preferred one for 0.016<G_t.

We also examined the vertical distribution of solid fraction at different locations in the horizontal direction for the preferred mixed solutions. Our general data at centers and at the nodes of the preferred subcritical mixed solutions in the form of certain general travelling rectangles-steady hexagons indicated that throughout the mushy layer the perturbation to solid fraction at the nodes is generally positive, while that at the centers of cells is generally negative. This general result holds irrespective of the parameter values considered, which indicates tendency for the chimney formation is higher at the cells' centers than at the nodes. Some typical results are presented in Figure 7 for the vertical

distribution of the basic state (graph labeled by a circle) and total solid fraction at both centers (graph labeled by a triangle) and the nodes (graphs labeled by a filled circle and a square) of the preferred subcritical down-mixed pattern, due to general travelling rectangles-steady hexagons, with b=0.46. In these calculation δ=0.2, G=1.25, G_t=0.008, K_1 =1.0, and the value ε= - 0.001 is chosen, which corresponds to the maximum value of $|\varepsilon|$=0.001 beyond which the solid fraction becomes negative. This is based on the physical ground that the value of the perturbation to the solid fraction cannot be such that total solid fraction becomes negative. It is seen from this figure that the tendency for chimney formation is higher at the lower boundary than anywhere else in the layer. Similar to the discussion provided in part 1 for the solid fraction due to the travelling mode, the non-vertical features of the chimneys and the compositional strips due to the travelling mode component discovered first by Anderson and Worster (1996) persist in the present parameter regime where the mixed solutions are preferred. Figure 8 presents the results for case presented in the figure 7 with the exception that here the data are for ε=0.001, so that the flow is upward at the cells' centers. It can be seen from the results presented in the figure 8 that here tendency for the chimney formation is highest at some interior location somewhat away from the lower boundary but still in the lower half of the mushy layer.

4. Conclusion and remarks

We investigated the problem of nonlinear convection, due to combined oscillatory and stationary modes, which are referred to as mixed modes, in horizontal mushy layers during the solidification of binary alloys. We considered particular range of the

parameter values where the critical values of the scaled Rayleigh number R for the onset of oscillatory and stationary convection are sufficiently close, and we developed and analyzed a nonlinear theory for the mixed modes of convection, which can be either subcritical or supercritical. Twelve new classes of nonlinear mixed solutions are detected. Six of these classes of solutions are subcritical and the other six classes are supercritical. For each class of solutions, the oscillatory components of the mixed modes, which could be either standing wave, simple travelling wave, or general travelling wave, depend on a parameter b in the range $|b| \leq 0.5$. Thus, within each class, there are infinite mixed solutions each of which corresponds to a particular value of b in its above domain. The main results for particular relevant range of the parameter values are provided for the preferred mixed solutions, which correspond to the lowest value of R. The preferred solutions are found to be subcritical and composed of steady hexagonal mode and general travelling rectangular mode, whose b values can lie in the range 0.44-0.46 depending on the precise range of the parameter values. It was found that in contrast to the simple types of either oscillatory solutions, where subcritical three-dimensional patterns cannot be possible (Riahi2002), or stationary solutions, where down-hexagons cannot be preferred (Amberg and Homsy1993), the preferred mixed solutions with down-flow at the cells' centers and up-flow at the cells' boundaries can be possible.

In regard to the relation of the present mixed-mode problem to those of simple-mode problems (Amberg and Homsy1993; Anderson and Worster1995; Riahi2002), it should be noted the range of applicability and restriction is each of these studies. Amberg and Homsy (1993) restricted their analysis to the case where the non-scaled original Stefan number $S_t=L/(C_L\Delta T)$ is an order one quantity and assumed that δ is of the same order as

ε, and they computed stationary solutions in the form of hexagons and rolls only. Their hexagonal solution was determined to order ε since R_{10} was non-zero to this order. However, R_{10} was zero for rolls, and so they carried out their analysis for rolls to order ε^2 to determine the solution for rolls. Their results indicated that $R_{10}<0$ for the steady hexagons, so that steady up-hexagons were subcritical, while steady down-hexagons were supercitical. Hence, the steady solution, which can correspond to the smallest value of R, was found to be that of up-hexagons. Anderson and Worster (1995) studied the case where the scaled Stefan number S is an order one quantity and assumed (3), and they also computed stationary solutions in the form hexagons and rolls only. Similar to the results obtained by Amberg and Homsy (1993), they found that $R_{10}<0$ for the steady hexagons and $R_{10}=0$ for the steady rolls. Hence, again the steady solution, which can correspond to the smallest value of R, is that of up-hexagons if the strict ordering condition $\varepsilon R_{10} >> \varepsilon\delta R_{11}$ is assumed. However, to explore the possibility for the preference of down-hexagons, which could bear some relevance with respect to the experimental observation (Tait et al.1992), Anderson and Worster (1995) found from their result that for K_1 of order δ to the leading term, then a range in the parameter values existed, where the steady down-hexagons can correspond to the smallest value of R, provided combined effect of $R_{10}+\delta R_{11}$ is taken into account. Riahi (2002) carried out nonlinear investigation for the simple oscillatory solutions in the particular range of the parameter values where the oscillatory convection can be preferred over the stationary convection. He found that $R_{10}=0$, so that no subcritical solution to order ε was possible. He then studied the problem to order ε^2 and found that all the solutions to this order were supercritical. The preferred oscillatory solutions, which can correspond to the smallest value of R, were

found to be that of simple travelling rolls (b =|0.5|) for most of the relevant range in G_t and standing rolls (b=0.0) for a very small intermediate range of values for G_t. The results of the present study for the mixed solutions indicated that the solutions in the form of combined steady hexagons and certain general travelling rectangles (b=0.44, 0.45, 0.46) can correspond to the lowest value of R. Since the value of b is close to that of a simple travelling component (b=0.5), it can be concluded that, to an approximation, the preferred mixed solution is a combination of the preferred stationary solution in the stationary domain (steady hexagons) and two sets of the preferred simple solution in the oscillatory domain (two sets of inclined simple travelling rolls, which can form simple travelling rectangles). This is the extent to which the preferred mixed solution can be related to the preferred simple solutions.

In regard to some extension of the present nonlinear mixed-modes theory, it should be noted that such an extension involves very lengthy and tedious analyses and studies of at least order ε^2 system, its corresponding solutions for R_{20}, order $\varepsilon\delta$ system, its corresponding solutions for ω_{11} since it turns out that R_{20} for the mixed solutions depend in general on the leading nonlinear contribution to the frequency, and the stability of all the solutions with respect to arbitrary three-dimensional disturbances. Although the preferred solutions of the present study are expected to be stable for sufficiently small ε, such extension of the present work could provide stable solutions at higher values of ε and so in a sense could complement the results of the present study. Present author presently carries out such extension and the results will be reported and published as a separate paper in near future.

The only available experimental observation known to author for the planform of weak convection and chimney formation in a mushy layer is that due to Tait et al. (1992). These authors solidified an ammonium chloride solution in a square tank by slow cooling. For their melt solution and experiment $\delta \approx 1$, $S \approx 5.0$ and $C \approx 20$, which implies $G \approx 1.25$ and $G_t \approx 0.008$. They were able to observe the flow structure near the onset of motion. They found that the flow pattern was roughly that of hexagons with down-flow at the cells' centers and up-flow mainly at the nodes of the cells. This observed flow features were in contrast to the theoretical results by Amberg and Homsy (1993), where preferred hexagonal cells were found to have up-flow at the cells' centers and down-flow at the cells' boundaries, and by Anderson and Worster (1995), where the preferred up-hexagons were predicted in a domain where down-hexagons were observed. Riahi (2002) carried out theoretical studies of weakly nonlinear convection in mushy layers for particular range of the parameter values where oscillatory modes were demonstrated to be the most critical ones. He showed that no preferred hexagonal convection was possible. As was demonstrated in part 1, for the parameter regime where the experimental observations are available, both stationary and oscillatory modes need to be taken into account to determine the preferred flow features. Hence, we undertook the present study as the first step to arrive at a reasonably complete theory for the weak convection in mushy layers. An important result of the present study is that of preference of mixed solutions in the form of general travelling rectangles-steady hexagons with down flow at the cells' centers and up-flow at the cells' boundaries in the parameter regime, where the available experiments were carried out. Despite some agreement of the present results with those of the experimental observations, there are still questions, which need to be

explained in regard to some disagreement of the present results with those observed such as up-flow along the nodes only, etc. We hope that further studies of the extension of the present theory to take into account both oscillatory and stationary modes could lead to further understanding the flow features in mushy layers and their relations with respect to the experimental observations.

Appendix

The system of equations and boundary conditions at order ε are given below

$$\{\Delta_2(-\nabla^2 V_{10}+R_{00}\theta_{10}+R_{10}\theta_{00})=K_1\{\nabla^2(\phi_{00}\Delta_2 V_{00})+(\partial/\partial z)[(\partial^2 V_{00}/\partial x\partial z)(\partial\phi_{00}/\partial x)+(\partial^2 V_{00}/\partial y\partial z)(\partial\phi_{00}/\partial y)+\pi^2 V_{00}(\partial\phi_{00}/\partial z)],$$

$$\nabla^2\theta_{10}+G(R_{00}\Delta_2 V_{10}+R_{10}\Delta_2 V_{00}+R_{00}\boldsymbol{\Omega}V_{00}.\nabla\theta_{00})=0,$$

$$S[(\partial/\partial t_1)-(\partial/\partial z)]\phi_{10}+\nabla^2\theta_{10}+R_{00}\Delta_2 V_{10}= -R_{10}\Delta_2 V_{00}-(S\omega_{11}/\omega_{01})\partial\phi_{00}/\partial t_1+R_{00}\boldsymbol{\Omega}V_{00}.\nabla\theta_{00},$$

$$V_{10}=\theta_{10}=0 \quad \text{at} \quad z=0,$$

$$V_{10}=\theta_{10}=\phi_{10}=0 \quad \text{at} \quad z=1,$$

where $t_1=\omega t/\omega_{01}\}$. (A1)

The solvability conditions for the system (A1) are reduced to the following two sets of equations:

$$R_{10}(|A_n^+|^2+|A_n^-|^2)=B\{2K_1\pi^4/[CG(\sqrt{G})(\pi^2-\omega_{01}^2)]\}\sum_{l,p}(1+\psi_{lp}^{(m)})\{H_p[A_n^+ A_l A_p^+ <\eta_l \eta_p^+ \eta_n^+>+A_n^- A_l A_p^+ <\eta_l \eta_p^+ \eta_n^->]+H_p^* [A_n^+ A_l A_p^- <\eta_l \eta_p^- \eta_n^+>+A_n^- A_l A_p^- <\eta_l \eta_p^- \eta_n^->]\}-B[3K_1\pi^2/(CG\sqrt{G})]\sum_{l,p}(1+\psi_{lp}^{(m)})\{A_n^+ A_p^+ A_l <\eta_p^+ \eta_l \eta_n^+>+A_n^- A_p^+ A_l <\eta_p^+ \eta_l \eta_n^->+A_n^+ A_p^- A_l <\eta_p^- \eta_l \eta_n^+>+A_n^- A_p^- A_l <\eta_p^- \eta_l \eta_n^->\},$$

$(n=-M,...,-1,1,...,M)$, (A2a)

$(R_{10}+\lambda_1)|A_n|^2B=\{2K_1\pi^4/[CG\,(\sqrt{G})(\pi^2-\omega_{01}{}^2)]\}\sum_{l,p=-M}^{M}(1+\psi_{lp}^{(o)})[H_p(A_n\,A_l^{+}\,A_p^{+}<\eta_n\,\eta_l^{+}\,\eta_p^{+}>+A_n\,A_l^{-}A_p^{+}<\eta_n\,\eta_l^{-}\,\eta_p^{+}>)+H_p^{*}(A_n\,A_l^{+}\,A_p^{-}<\eta_n\,\eta_l^{+}\,\eta_p^{-}>+A_n\,A_l^{-}\,A_p^{-}<\eta_n\,\eta_l^{-}\,\eta_p^{-}>)]-B\,[3K_1\,\pi^2/(CG\sqrt{G})]\sum\,(1+\psi_{lp}^{(s)})A_n\,A_l\,A_p<\eta_n\,\eta_l\,\eta_p>$, $(n=-N,\ \ ,-1,1,...,M)$, (A2b)

where

$H_p=-10iS_p\omega_{01}/(3\pi^2)+[iS_p\omega_{01}/(4\pi)][\exp(-iS_p\omega_{01})]\{4\pi[1-\cos(\omega_{01})]/(4\pi^2-\omega_{01}{}^2)-4\,\pi i\,\sin(\omega_{01}\,S_p)/(4\pi^2-\omega_{01}{}^2)\}-(3/2)[1-\exp(-i\,\omega_{01}S_p)]/(i\,\omega_{01}S_p)+(3/4)[\exp(-i\,\omega_{01}S_p)]\{-2\omega_{01}S_p\sin(\omega_{01}S_p)/(4\pi^2-\omega_{01}{}^2)-2i\,\omega_{01}S_p[1-\cos(\omega_{01})]/(4\pi^2-\omega_{01}{}^2)\}$, (A2c)

$\psi_{lp}^{(o)}=\mathbf{a}_l^{(o)}.\mathbf{a}_p^{(o)}/\pi^2$, $\psi_{lp}^{(m)}=\mathbf{a}_l^{(s)}.\mathbf{a}_p^{(o)}/\pi^2$, $\psi_{lp}^{(s)}=\mathbf{a}_l^{(s)}.\mathbf{a}_p^{(s)}/\pi^2$, (A2d)

and the summations in the right-hand-side in (A2a) for l and p run from –N to N and –M to M, respectively.

The expressions for the coefficients $C_i^{(j)}$ (i=1, 2, 3; j=1, 2, 3, 4, 5, 6) introduced in (19) for the simple travelling-steady class of the detected mixed solutions are given below

$C_1^{(1)}=(D_1C_0/2-D_2)/\sqrt{6}$, $C_2^{(1)}=D_1C_0/\sqrt{6}$, $C_3^{(1)}=D_2/\sqrt{6}$, $D_1\equiv 2K_1\pi^4/[CG(\pi^2-\omega_{01}{}^2)\sqrt{G}]$, $D_2\equiv 3K_1\pi^2/(CG\sqrt{G})$, $C_0\equiv-(\sin\omega_{01}/\omega_{01})[3+\omega_{01}/(4\pi^2-\omega_{01}{}^2)]$, (A3a)

$C_1^{(2)}=C_1^{(1)}/2$, $C_2^{(2)}=3C_2^{(1)}/4$, $C_3^{(2)}=C_3^{(1)}/2$, (A3b)

$C_1^{(3)}=D_1C_0/4-D_2/2$, $C_2^{(3)}=D_1C_0/3$, $C_3^{(3)}=0.0$, (A3c)

$C_1^{(4)}=D_1C_0/8-D_2/4$, $C_2^{(4)}=D_1C_0/2$, $C_3^{(4)}=0.0$, (A3d)

$C_1^{(5)}=D_1C_0/(4\sqrt{2})-D_2/\sqrt{8}$, $C_2^{(5)}=D_1C_0/(3\sqrt{2})$, $C_3^{(5)}=0.0$, (A3e)

$C_1^{(6)}=C_1^{(5)}$, $C_2^{(6)}=C_2^{(5)}$, $C_3^{(6)}=0.0$. (A3f)

The expressions for the coefficients $C_i^{(j)}$(i=1, 2, 3; j=7, 8, 9, 10, 11, 12) of the standing wave-steady class of the mixed solutions numbers 7 through 12 are given below

$C_1^{(7)}=D_1C_0/(\sqrt{6})-2D_2/\sqrt{6}$, $C_2^{(7)}=2D_1C_0/\sqrt{6}$, $C_3^{(7)}=-D_2/\sqrt{6}$, (A4a)

$C_1^{(8)}=D_1C_0/(2\sqrt{6})-D_2/(\sqrt{6})$, $C_2^{(8)}=D_1C_0\sqrt{6}/2$, $C_3^{(8)}=-D_2/\sqrt{6}$, (A4b)

$C_1^{(9)}=D_1C_0/4-D_2/2$, $C_2^{(9)}=D_1C_0/3$, $C_3^{(9)}=0.0$, (A4c)

$C_1^{(10)}=C_1^{(9)}$, $C_2^{(10)}=D_1C_0/2$, $C_3^{(10)}=0.0$, (A4d)

$C_1^{(11)}=D_1C_0\sqrt{2}/4-D_2/\sqrt{2}$, $C_2^{(11)}=D_1C_0\sqrt{2}/3$, $C_3^{(11)}=0.0$, (A4e)

$C_1^{(12)}=C_1^{(11)}$, $C_2^{(12)}=D_1C_0/\sqrt{2}$, $C_3^{(12)}=0.0$. (A4f)

The expressions for the coefficients C (i=1, 2, 3; j=13, 14, 15, 16, 17, 18) introduced in (19) for the general travelling-steady class of the detected mixed solutions are given below

$C_1^{(13)}=D_1C_0b_1/(2\sqrt{6})-D_2b_1/\sqrt{6}$, $C_2^{(13)}=D_1C_0b_1/\sqrt{6}$, $C_3^{(13)}=-D_2/\sqrt{6}$, $b_1\equiv1+2(0.25-b)^{0.5}$, (A5a)

$C_1^{(14)}=C_1^{(13)}/2$, $C_2^{(14)}=(\sqrt{6})D_1C_0b_1/4$, $C_3^{(14)}=C_3^{(13)}$, (A5b)

$C_1^{(15)}=D_1C_0b_1/8-D_2b_1/4$, $C_2^{(15)}=D_1C_0b_1$, $C_3^{(15)}=0.0$, (A5c)

$C_1^{(16)}=C_1^{(15)}$, $C_2^{(16)}=C_2^{(15)}/4$, $C_3^{(16)}=0.0$, (A5d)

$C_1^{(17)}=D_1C_0b_1/(4\sqrt{2})-D_2b_1/\sqrt{8}$, $C_2^{(17)}=D_1C_0b_1/(3\sqrt{2})$, $C_3^{(17)}=0.0$, (A5e)

$C_1^{(18)}=C_1^{(17)}$, $C_2^{(18)}=D_1C_0b_1/\sqrt{8}$, $C_3^{(18)}=0.0$. (A5f)

REFERENCES

AMBERG, G. AND HOMSY, G. M. 1993 Nonlinear analysis of buoyant convection in binary solidification with application to channel formation. J. Fluid Mech. **252**, 79-98.

ANDERSON, D. M. AND WORSTER, M. G. 1995 Weakly nonlinear analysis of convection in mushy layers during the solidification of binary alloys. J. Fluid Mech. **302**, 307-331.

ANDERSON, D. M. AND WORSTER, M. G. 1996 A new oscillatory instability in a mushy layer during the solidification of binary alloys. J. Fluid Mech. **307**, 245-267.

BUSSE, F. H. 1967 The stability of finite amplitude convection and its relation to an extremum principal. J. Fluid Mech. **30**, 625-649.

BUSSE, F. H. 1975 Patterns of convection in spherical shells. J. Fluid Mech. **72**, 67-85.

BUSSE, F. H. AND RIAHI, D. N. 1988 Mixed-mode patterns of bifurcations from spherically symmetric basic states. Nonlinearity **1**, 379-388.

RIAHI, D. N. 1985 Nonlinear convection in a porous layer with finite conducting boundaries. J. Fluid Mech. **129**, 153-171.

RIAHI, D. N. 2002 On nonlinear convection in mushy layers. Part1. Oscillatory modes of convection. J. Fluid Mech. **467**, 331-359.

TAIT, S., JAHRLING, K. AND JAUPART, C. 1992 The planform of compositional convection and chimney formation in a mushy layer. Nature **359**, 406-408.

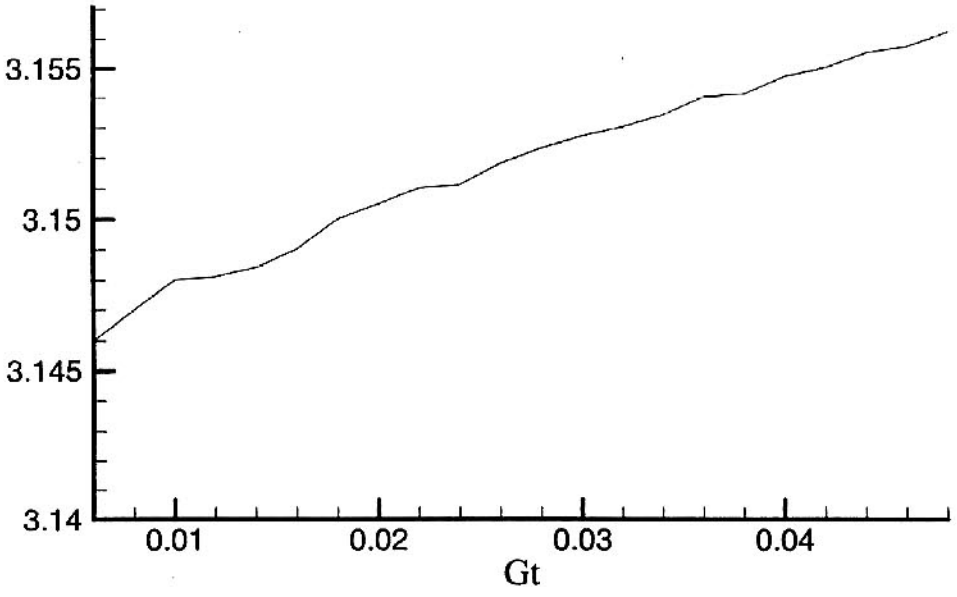

Figure 1. The frequency ω_{01} versus G_t.

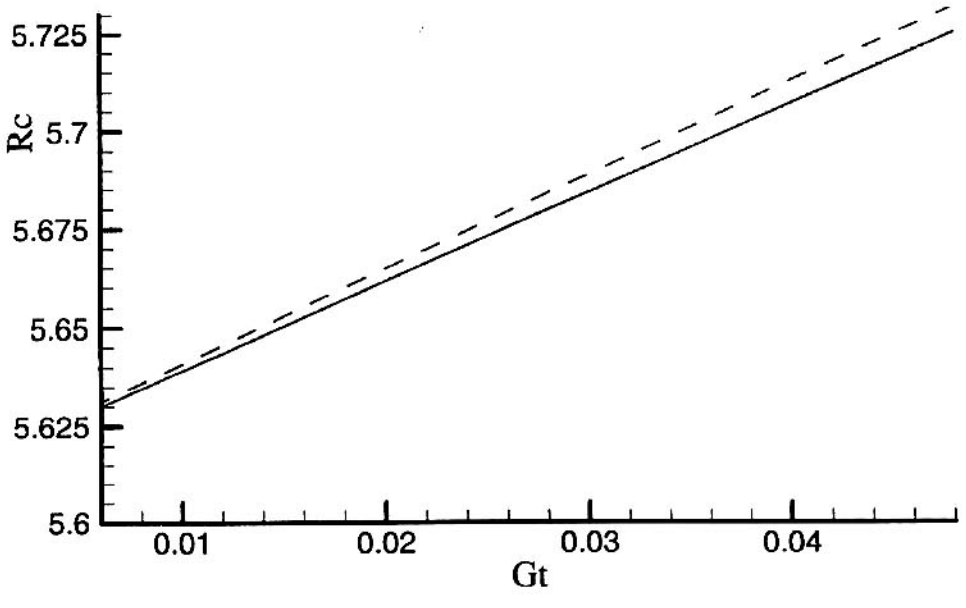

Figure 2. The critical values of the scaled Rayleigh numbers $R_c^{(o)}$ (solid line) and $R_c^{(s)}$ (dashed line) versus G_t for G=1.25, K_1=1.0 and δ=0.2.

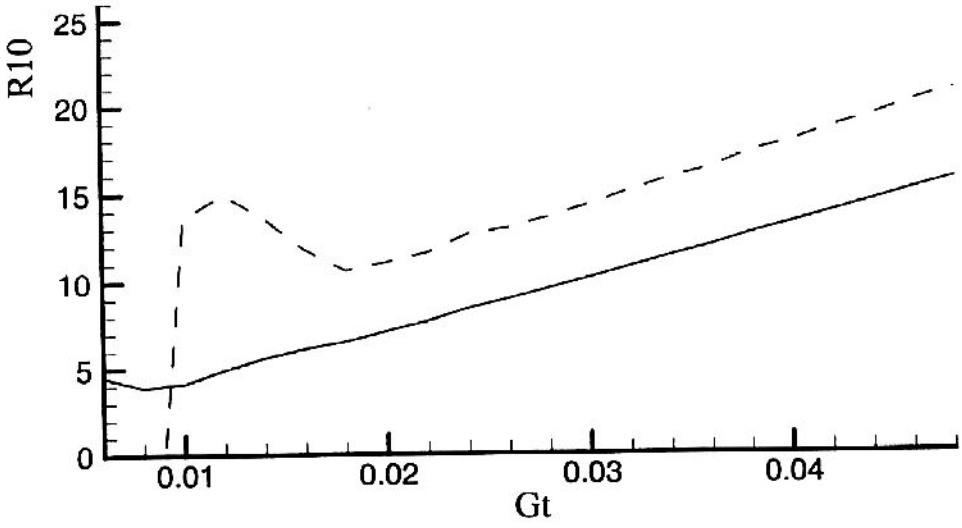

Figure 3. R_{10} versus G_t for subcritical flow in the form of certain general travelling rectangle-steady hexagons. Here G=1.25, K_1=1.0 and $R=R_c^{(o)}-1.0$. The solid line and dashed line correspond to b=0.45 and 0.46, respectively.

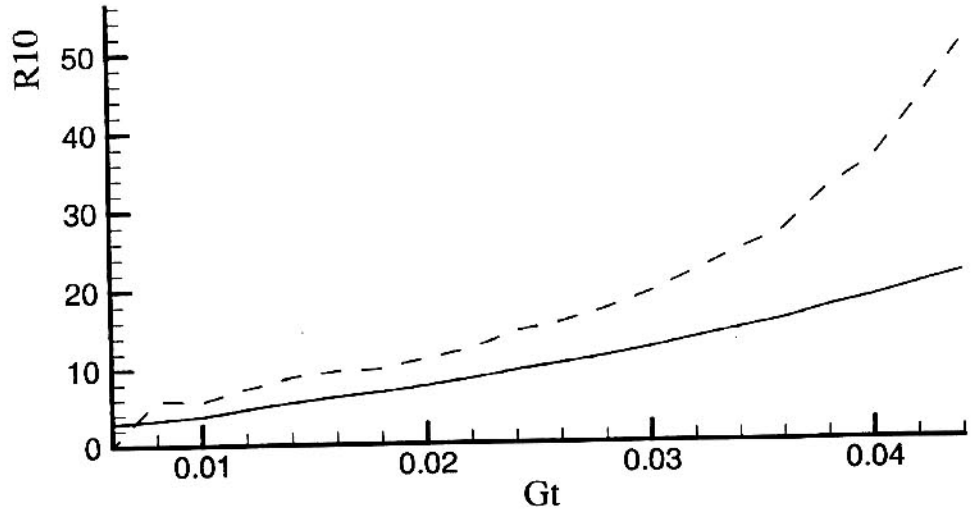

Figure 4. R_{10} versus G_t for subcritical flow in the form of certain general travelling rectangle-steady hexagons. Here G=1.25, K_1=1.0 and $R=R_c^{(o)}-0.1$. The solid line and dashed line correspond to b=0.44 and 0.45, respectively.

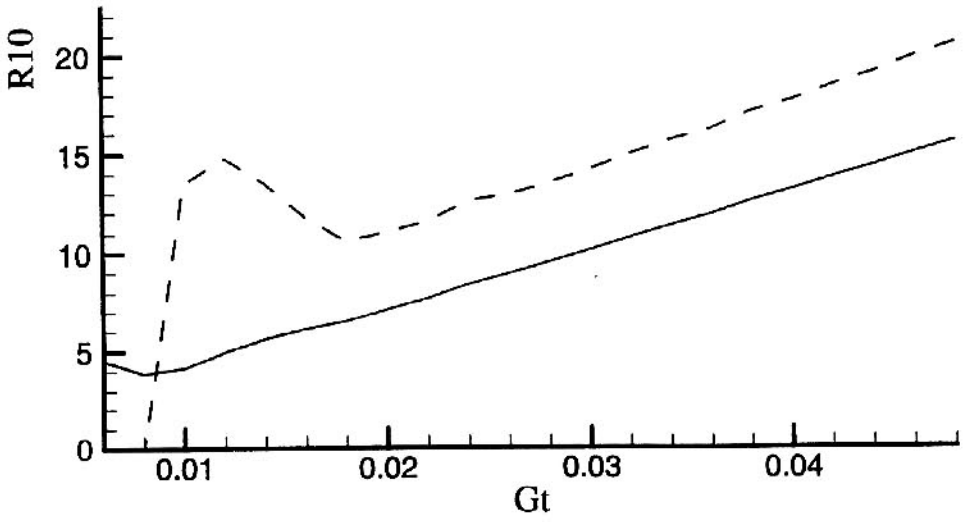

Figure 5. R_{10} versus G_t for subcritical flow in the form of certain general travelling rectangle-steady hexagons. Here G=1.25, K_1=1.0 and R=4.6. The solid line and dashed line correspond to b=0.45 and 0.46, respectively.

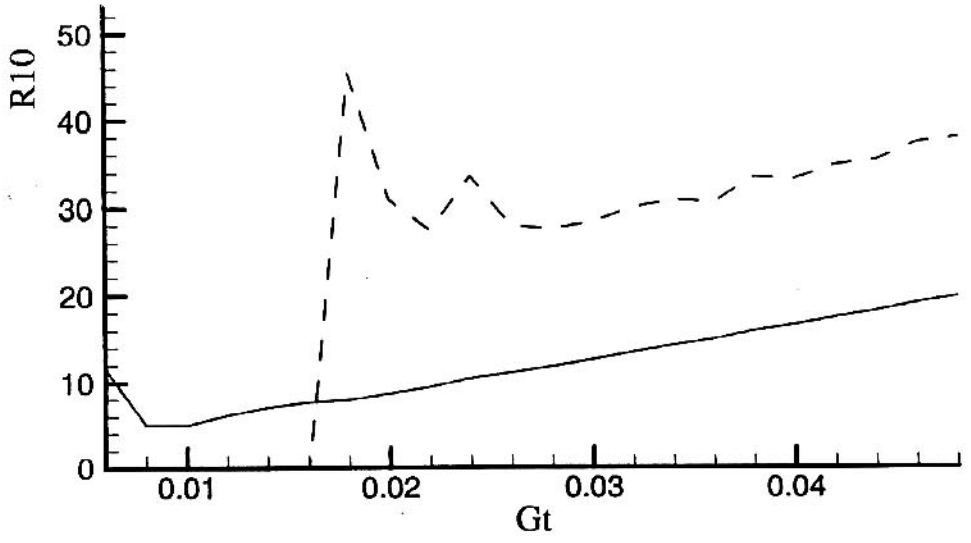

Figure 6. R_{10} versus G_t for subcritical flow in the form of certain general travelling rectangle-steady hexagons. Here G=1.25, K_1=1.0 and R=5.5. The solid line and dashed line correspond to b=0.45 and 0.46, respectively.

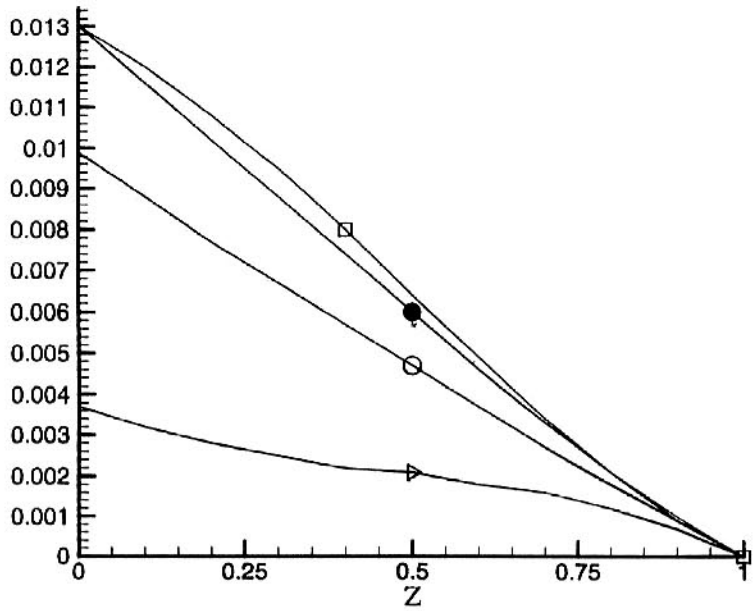

Figure 7. Solid fraction versus z for the preferred subcritical down-mixed pattern in the form of general travelling rectangle-steady hexagons with b=0.46, G=1.25, G_t=0.008 and K_1=1.0. Here graphs labeled by the symbols of circle, triangle, filled circle and square present, respectively, the basic solid fraction ϕ_B, $\tilde{\phi}$ (x =y =t =0.0), $\tilde{\phi}$ (x = 4/3, y = t=0.0) and $\tilde{\phi}$ (x = 4/3, y =0, t =1.0).

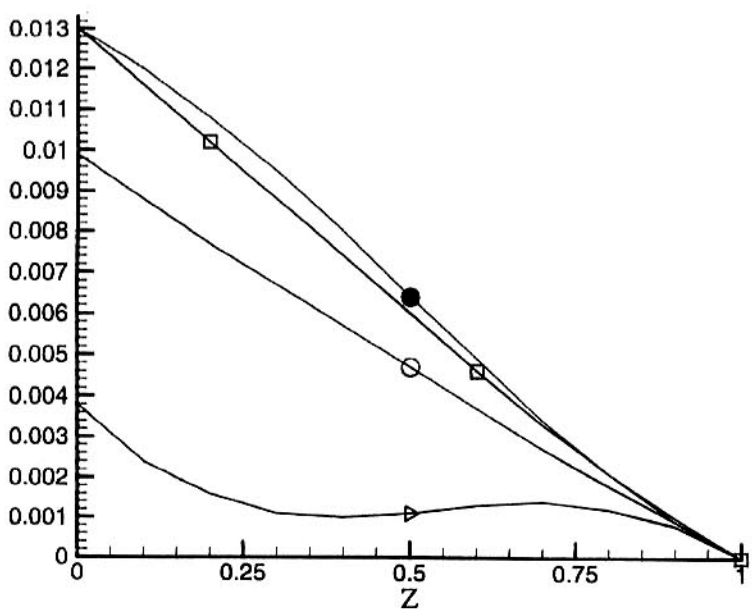

Figure 8. Solid fraction versus z for the preferred subcritical up-mixed pattern in the form of general travelling rectangle-steady hexagons with b=0.46, G=1.25, G_t=0.008 and K_1=1.0. Here graphs labeled by the symbols of circle, triangle, filled circle and square present, respectively, the basic solid fraction ϕ_B, $\tilde{\phi}$ (x =y =t =0.0), $\tilde{\phi}$ (x =4/3, y =t =0.0) and $\tilde{\phi}$ (x =4/3, y =0, t =1.0).

List of Recent TAM Reports

No.	Authors	Title	Date
922	Nimmagadda, P. B. R., and P. Sofronis	Leading order asymptotics at sharp fiber corners in creeping-matrix composite materials	Oct. 1999
923	Yoo, S., and D. N. Riahi	Effects of a moving wavy boundary on channel flow instabilities—*Theoretical and Computational Fluid Dynamics* (submitted)	Nov. 1999
924	Adrian, R. J., C. D. Meinhart, and C. D. Tomkins	Vortex organization in the outer region of the turbulent boundary layer—*Journal of Fluid Mechanics* **422**, 1–53 (2000)	Nov. 1999
925	Riahi, D. N., and A. T. Hsui	Finite amplitude thermal convection with variable gravity—*International Journal of Mathematics and Mathematical Sciences* **25**, 153–165 (2001)	Dec. 1999
926	Kwok, W. Y., R. D. Moser, and J. Jiménez	A critical evaluation of the resolution properties of *B*-spline and compact finite difference methods—*Journal of Computational Physics* (submitted)	Feb. 2000
927	Ferry, J. P., and S. Balachandar	A fast Eulerian method for two-phase flow—*International Journal of Multiphase Flow*, in press (2000)	Feb. 2000
928	Thoroddsen, S. T., and K. Takehara	The coalescence–cascade of a drop—*Physics of Fluids* **12**, 1257–1265 (2000)	Feb. 2000
929	Liu, Z.-C., R. J. Adrian, and T. J. Hanratty	Large-scale modes of turbulent channel flow: Transport and structure—*Journal of Fluid Mechanics* **448**, 53–80 (2001)	Feb. 2000
930	Borodai, S. G., and R. D. Moser	The numerical decomposition of turbulent fluctuations in a compressible boundary layer—*Theoretical and Computational Fluid Dynamics* (submitted)	Mar. 2000
931	Balachandar, S., and F. M. Najjar	Optimal two-dimensional models for wake flows—*Physics of Fluids*, in press (2000)	Mar. 2000
932	Yoon, H. S., K. V. Sharp, D. F. Hill, R. J. Adrian, S. Balachandar, M. Y. Ha, and K. Kar	Integrated experimental and computational approach to simulation of flow in a stirred tank—*Chemical Engineering Sciences* **56**, 6635–6649 (2001)	Mar. 2000
933	Sakakibara, J., Hishida, K., and W. R. C. Phillips	On the vortical structure in a plane impinging jet—*Journal of Fluid Mechanics* **434**, 273–300 (2001)	Apr. 2000
934	Phillips, W. R. C.	Eulerian space–time correlations in turbulent shear flows—*Physics of Fluids* **12**, 2056–2064 (2000)	Apr. 2000
935	Hsui, A. T., and D. N. Riahi	Onset of thermal–chemical convection with crystallization within a binary fluid and its geological implications—*Geochemistry, Geophysics, Geosystems* **2**, 2000GC000075 (2001)	Apr. 2000
936	Cermelli, P., E. Fried, and S. Sellers	Configurational stress, yield, and flow in rate-independent plasticity—*Proceedings of the Royal Society of London A* **457**, 1447–1467 (2001)	Apr. 2000
937	Adrian, R. J., C. Meneveau, R. D. Moser, and J. J. Riley	Final report on 'Turbulence Measurements for Large-Eddy Simulation' workshop	Apr. 2000
938	Bagchi, P., and S. Balachandar	Linearly varying ambient flow past a sphere at finite Reynolds number—Part 1: Wake structure and forces in steady straining flow	Apr. 2000
939	Gioia, G., A. DeSimone, M. Ortiz, and A. M. Cuitiño	Folding energetics in thin-film diaphragms—*Proceedings of the Royal Society of London A* **458**, 1223–1229 (2002)	Apr. 2000
940	Chaïeb, S., and G. H. McKinley	Mixing immiscible fluids: Drainage induced cusp formation	May 2000
941	Thoroddsen, S. T., and A. Q. Shen	Granular jets—*Physics of Fluids* **13**, 4–6 (2001)	May 2000
942	Riahi, D. N.	Non-axisymmetric chimney convection in a mushy layer under a high-gravity environment—In *Centrifugal Materials Processing* (L. L. Regel and W. R. Wilcox, eds.), 295–302 (2001)	May 2000

List of Recent TAM Reports (cont'd)

No.	Authors	Title	Date
943	Christensen, K. T., S. M. Soloff, and R. J. Adrian	PIV Sleuth: Integrated particle image velocimetry interrogation/validation software	May 2000
944	Wang, J., N. R. Sottos, and R. L. Weaver	Laser induced thin film spallation—*Experimental Mechanics* (submitted)	May 2000
945	Riahi, D. N.	Magnetohydrodynamic effects in high gravity convection during alloy solidification—In *Centrifugal Materials Processing* (L. L. Regel and W. R. Wilcox, eds.), 317–324 (2001)	June 2000
946	Gioia, G., Y. Wang, and A. M. Cuitiño	The energetics of heterogeneous deformation in open-cell solid foams—*Proceedings of the Royal Society of London A* **457**, 1079–1096 (2001)	June 2000
947	Kessler, M. R., and S. R. White	Self-activated healing of delamination damage in woven composites—*Composites A: Applied Science and Manufacturing* **32**, 683–699 (2001)	June 2000
948	Phillips, W. R. C.	On the pseudomomentum and generalized Stokes drift in a spectrum of rotational waves—*Journal of Fluid Mechanics* **430**, 209–229 (2001)	July 2000
949	Hsui, A. T., and D. N. Riahi	Does the Earth's nonuniform gravitational field affect its mantle convection?—*Physics of the Earth and Planetary Interiors* (submitted)	July 2000
950	Phillips, J. W.	Abstract Book, 20th International Congress of Theoretical and Applied Mechanics (27 August – 2 September, 2000, Chicago)	July 2000
951	Vainchtein, D. L., and H. Aref	Morphological transition in compressible foam—*Physics of Fluids* **13**, 2152–2160 (2001)	July 2000
952	Chaïeb, S., E. Sato-Matsuo, and T. Tanaka	Shrinking-induced instabilities in gels	July 2000
953	Riahi, D. N., and A. T. Hsui	A theoretical investigation of high Rayleigh number convection in a nonuniform gravitational field—*Acta Mechanica* (submitted)	Aug. 2000
954	Riahi, D. N.	Effects of centrifugal and Coriolis forces on a hydromagnetic chimney convection in a mushy layer—*Journal of Crystal Growth* **226**, 393–405 (2001)	Aug. 2000
955	Fried, E.	An elementary molecular-statistical basis for the Mooney and Rivlin–Saunders theories of rubber-elasticity—*Journal of the Mechanics and Physics of Solids* **50**, 571–582 (2002)	Sept. 2000
956	Phillips, W. R. C.	On an instability to Langmuir circulations and the role of Prandtl and Richardson numbers—*Journal of Fluid Mechanics* **442**, 335–358 (2001)	Sept. 2000
957	Chaïeb, S., and J. Sutin	Growth of myelin figures made of water soluble surfactant—Proceedings of the 1st Annual International IEEE–EMBS Conference on Microtechnologies in Medicine and Biology (October 2000, Lyon, France), 345–348	Oct. 2000
958	Christensen, K. T., and R. J. Adrian	Statistical evidence of hairpin vortex packets in wall turbulence—*Journal of Fluid Mechanics* **431**, 433–443 (2001)	Oct. 2000
959	Kuznetsov, I. R., and D. S. Stewart	Modeling the thermal expansion boundary layer during the combustion of energetic materials—*Combustion and Flame*, in press (2001)	Oct. 2000
960	Zhang, S., K. J. Hsia, and A. J. Pearlstein	Potential flow model of cavitation-induced interfacial fracture in a confined ductile layer—*Journal of the Mechanics and Physics of Solids*, **50**, 549–569 (2002)	Nov. 2000
961	Sharp, K. V., R. J. Adrian, J. G. Santiago, and J. I. Molho	Liquid flows in microchannels—Chapter 6 of *CRC Handbook of MEMS* (M. Gad-el-Hak, ed.) (2001)	Nov. 2000
962	Harris, J. G.	Rayleigh wave propagation in curved waveguides—*Wave Motion*, in press (2001)	Jan. 2001

List of Recent TAM Reports (cont'd)

No.	Authors	Title	Date
963	Dong, F., A. T. Hsui, and D. N. Riahi	A stability analysis and some numerical computations for thermal convection with a variable buoyancy factor—*Journal of Theoretical and Applied Mechanics*, in press (2002)	Jan. 2001
964	Phillips, W. R. C.	Langmuir circulations beneath growing or decaying surface waves—*Journal of Fluid Mechanics* (submitted)	Jan. 2001
965	Bdzil, J. B., D. S. Stewart, and T. L. Jackson	Program burn algorithms based on detonation shock dynamics—*Journal of Computational Physics* (submitted)	Jan. 2001
966	Bagchi, P., and S. Balachandar	Linearly varying ambient flow past a sphere at finite Reynolds number: Part 2—Equation of motion—*Journal of Fluid Mechanics* (submitted)	Feb. 2001
967	Cermelli, P., and E. Fried	The evolution equation for a disclination in a nematic fluid—*Proceedings of the Royal Society A* **458**, 1–20 (2002)	Apr. 2001
968	Riahi, D. N.	Effects of rotation on convection in a porous layer during alloy solidification—Chapter 12 in *Transport Phenomena in Porous Media* (D. B. Ingham and I. Pop, eds.), 316–340 (2002)	Apr. 2001
969	Damljanovic, V., and R. L. Weaver	Elastic waves in cylindrical waveguides of arbitrary cross section—*Journal of Sound and Vibration* (submitted)	May 2001
970	Gioia, G., and A. M. Cuitiño	Two-phase densification of cohesive granular aggregates—*Physical Review Letters* **88**, 204302 (2002) (in extended form and with added co-authors S. Zheng and T. Uribe)	May 2001
971	Subramanian, S. J., and P. Sofronis	Calculation of a constitutive potential for isostatic powder compaction—*International Journal of Mechanical Sciences* (submitted)	June 2001
972	Sofronis, P., and I. M. Robertson	Atomistic scale experimental observations and micromechanical/ continuum models for the effect of hydrogen on the mechanical behavior of metals—*Philosophical Magazine* (submitted)	June 2001
973	Pushkin, D. O., and H. Aref	Self-similarity theory of stationary coagulation—*Physics of Fluids* **14**, 694–703 (2002)	July 2001
974	Lian, L., and N. R. Sottos	Stress effects in ferroelectric thin films—*Journal of the Mechanics and Physics of Solids* (submitted)	Aug. 2001
975	Fried, E., and R. E. Todres	Prediction of disclinations in nematic elastomers—*Proceedings of the National Academy of Sciences* **98**, 14773–14777 (2001)	Aug. 2001
976	Fried, E., and V. A. Korchagin	Striping of nematic elastomers—*International Journal of Solids and Structures* **39**, 3451–3467 (2002)	Aug. 2001
977	Riahi, D. N.	On nonlinear convection in mushy layers: Part I. Oscillatory modes of convection—*Journal of Fluid Mechanics* **467**, 331–359 (2002)	Sept. 2001
978	Sofronis, P., I. M. Robertson, Y. Liang, D. F. Teter, and N. Aravas	Recent advances in the study of hydrogen embrittlement at the University of Illinois—Invited paper, Hydrogen–Corrosion Deformation Interactions (Sept. 16–21, 2001, Jackson Lake Lodge, Wyo.)	Sept. 2001
979	Fried, E., M. E. Gurtin, and K. Hutter	A void-based description of compaction and segregation in flowing granular materials—*Proceedings of the Royal Society of London A* (submitted)	Sept. 2001
980	Adrian, R. J., S. Balachandar, and Z.-C. Liu	Spanwise growth of vortex structure in wall turbulence—*Korean Society of Mechanical Engineers International Journal* **15**, 1741–1749 (2001)	Sept. 2001
981	Adrian, R. J.	Information and the study of turbulence and complex flow—*Japanese Society of Mechanical Engineers Journal B*, in press (2002)	Oct. 2001
982	Adrian, R. J., and Z.-C. Liu	Observation of vortex packets in direct numerical simulation of fully turbulent channel flow—*Journal of Visualization*, in press (2002)	Oct. 2001
983	Fried, E., and R. E. Todres	Disclinated states in nematic elastomers—*Journal of the Mechanics and Physics of Solids* **50**, 2691–2716 (2002)	Oct. 2001
984	Stewart, D. S.	Towards the miniaturization of explosive technology—Proceedings of the 23rd International Conference on Shock Waves (2001)	Oct. 2001
985	Kasimov, A. R., and Stewart, D. S.	Spinning instability of gaseous detonations—*Journal of Fluid Mechanics* (submitted)	Oct. 2001

List of Recent TAM Reports (cont'd)

No.	*Authors*	*Title*	*Date*
986	Brown, E. N., N. R. Sottos, and S. R. White	Fracture testing of a self-healing polymer composite—*Experimental Mechanics* (submitted)	Nov. 2001
987	Phillips, W. R. C.	Langmuir circulations—*Surface Waves* (J. C. R. Hunt and S. Sajjadi, eds.), in press (2002)	Nov. 2001
988	Gioia, G., and F. A. Bombardelli	Scaling and similarity in rough channel flows—*Physical Review Letters* **88**, 014501 (2002)	Nov. 2001
989	Riahi, D. N.	On stationary and oscillatory modes of flow instabilities in a rotating porous layer during alloy solidification—*Journal of Porous Media*, in press (2002)	Nov. 2001
990	Okhuysen, B. S., and D. N. Riahi	Effect of Coriolis force on instabilities of liquid and mushy regions during alloy solidification—*Physics of Fluids* (submitted)	Dec. 2001
991	Christensen, K. T., and R. J. Adrian	Measurement of instantaneous Eulerian acceleration fields by particle-image accelerometry: Method and accuracy—*Experimental Fluids* (submitted)	Dec. 2001
992	Liu, M., and K. J. Hsia	Interfacial cracks between piezoelectric and elastic materials under in-plane electric loading—*Journal of the Mechanics and Physics of Solids* (submitted)	Dec. 2001
993	Panat, R. P., S. Zhang, and K. J. Hsia	Bond coat surface rumpling in thermal barrier coatings—*Acta Materialia*, in press (2002)	Jan. 2002
994	Aref, H.	A transformation of the point vortex equations—*Physics of Fluids* **14**, 2395–2401 (2002)	Jan. 2002
995	Saif, M. T. A, S. Zhang, A. Haque, and K. J. Hsia	Effect of native Al_2O_3 on the elastic response of nanoscale aluminum films—*Acta Materialia* **50**, 2779–2786 (2002)	Jan. 2002
996	Fried, E., and M. E. Gurtin	A nonequilibrium theory of epitaxial growth that accounts for surface stress and surface diffusion—*Journal of the Mechanics and Physics of Solids*, in press (2002)	Jan. 2002
997	Aref, H.	The development of chaotic advection—*Physics of Fluids* **14**, 1315–1325 (2002); see also *Virtual Journal of Nanoscale Science and Technology*, 11 March 2002	Jan. 2002
998	Christensen, K. T., and R. J. Adrian	The velocity and acceleration signatures of small-scale vortices in turbulent channel flow—*Journal of Turbulence*, in press (2002)	Jan. 2002
999	Riahi, D. N.	Flow instabilities in a horizontal dendrite layer rotating about an inclined axis—*Proceedings of the Royal Society of London A* (submitted)	Feb. 2002
1000	Kessler, M. R., and S. R. White	Cure kinetics of ring-opening metathesis polymerization of dicyclopentadiene—*Journal of Polymer Science A* **40**, 2373–2383 (2002)	Feb. 2002
1001	Dolbow, J. E., E. Fried, and A. Q. Shen	Point defects in nematic gels: The case for hedgehogs—*Proceedings of the National Academy of Sciences* (submitted)	Feb. 2002
1002	Riahi, D. N.	Nonlinear steady convection in rotating mushy layers—*Journal of Fluid Mechanics* (submitted)	Mar. 2002
1003	Carlson, D. E., E. Fried, and S. Sellers	The totality of soft-states in a neo-classical nematic elastomer—*Proceedings of the Royal Society A* (submitted)	Mar. 2002
1004	Fried, E., and R. E. Todres	Normal-stress differences and the detection of disclinations in nematic elastomers—*Journal of Polymer Science B: Polymer Physics*, in **40**, 2098–2106 (2002)	June 2002
1005	Fried, E., and B. C. Roy	Gravity-induced segregation of cohesionless granular mixtures—*Lecture Notes in Mechanics*, in press (2002)	July 2002
1006	Tomkins, C. D., and R. J. Adrian	Spanwise structure and scale growth in turbulent boundary layers—*Journal of Fluid Mechanics* (submitted)	Aug. 2002
1007	Riahi, D. N.	On nonlinear convection in mushy layers: Part 2. Mixed oscillatory and stationary modes of convection—*Journal of Fluid Mechanics* (submitted)	Sept. 2002